Unraveling orbital hybridization of triplet emitters at the metal-organic interface

Pascal R. Ewen,[1] Jan Sanning,[1] Nikos L. Doltsinis,[2] Matteo Mauro,[3] Cristian A. Strassert,[1,*] and Daniel Wegner[1,†]

[1] *Physikalisches Institut and Center for Nanotechnology (CeNTech), Westfälische Wilhelms-Universität Münster, 48149 Münster, Germany*

[2] *Institut für Festkörpertheorie, Westfälische Wilhelms-Universität Münster, 48149 Münster, Germany*

[3] *Laboratoire de Chimie et des Biomatériaux Supramoléculaires, Institut de Science et d'Ingénierie Supramoléculaires (ISIS), Université de Strasbourg, 67083 Strasbourg, France*

(Dated: November 14, 2013)

We have investigated the structural and electronic properties of phosphorescent planar platinum(II) complexes at the interface of Au(111) with submolecular resolution using combined scanning tunneling microscopy and spectroscopy as well as density functional theory. Our analysis shows that molecule-substrate coupling and lateral intermolecular interactions are weak. While the ligand orbitals remain essentially unchanged upon contact to the substrate, we found modified electronic behavior at the Pt atom due to local hybridization and charge transfer to the substrate. Thus, this novel class of phosphorescent molecules exhibits well-defined and tunable interaction with its local environment.

PACS numbers: 68.37.Ef, 68.55.-a, 73.20.Hb, 81.07.Pr

Organic light emitting diodes (OLEDs) are currently investigated extensively as alternative, highly efficient lighting sources and for display technologies [1]. While pure organic emitters are limited to a quantum efficiency of 25% by fluorescence from excited singlet states, the introduction of a heavy-metal atom with large spin-orbit coupling can increase the efficiency up to 100% by triplet harvesting and phosphorescence [2, 3]. By far, most research and applications have concentrated on iridium(III) complexes that require octahedral coordination of the Ir atom [4]. Interactions of an Ir complex with its local environment lack defined directionality and are thus barely controllable, which usually leads to quenching effects and reduced quantum efficiencies when the Ir-complex loading in an OLED is too high [5]. In contrast, recently synthesized platinum(II) complexes not only yield quantum efficiencies of more than 85%, but they also exhibit no quenching effects even when aggregated into fibers or gels [6, 7]. The planar geometry enables well-defined interactions with the local environment that should be tunable.

The electronic properties of triplet emitters at conductive interfaces is fundamental for the understanding of electroluminescent devices, in particular light-emitting electrochemical cells (LEECs) and OLEDs. Scanning tunneling microscopy (STM) is an ideal tool to study single molecules in a conductive environment with high spatial resolution, while spectroscopic mapping via scanning tunneling spectroscopy (STS) can identify energetic positions and spatial distributions of molecular frontier orbitals [8–12]. Surprisingly, so far only few studies have used scanning probe techniques to study triplet emitters at the nanoscale [13–15], and none of them have utilized the advantages of combined STM and STS.

We report on a combined STM and STS study of two Pt-based triplet emitters at the interface of Au(111). We found that the molecules self-assemble into densely-packed monolayers. Through local STS spectra and energy-resolved spectroscopic maps we identified various occupied and unoccupied frontier orbitals. Comparison with density functional theory (DFT) reveals that intermolecular interactions as well as the coupling of the ligand to the substrate are relatively weak. However, we found modified electronic behavior at the Pt atom, which we attribute to hybridization with the Au surface leading to partial depopulation of the Pt d_{z^2}-orbital. The molecular coupling with its local environment is thus well-defined and offers opportunities for controlled tuning of electronic and optical properties of this type of phosphorescent complexes.

All experiments were performed under ultra-high vacuum (UHV) conditions (base pressure $1 \cdot 10^{-10}$ mbar) using a commercial low-temperature STM (Createc LT-STM). The synthesis of pyridine 2,6-bis(3-(trifluoromethyl)-1,2,4-triazolato-5-yl)pyridine platinum(II) (Pt-H) and 4-pentyl-pyridine 2,6-bis(3-(trifluoromethyl)-1,2,4-triazolato-5-yl)pyridine platinum(II) (Pt-amyl) is described elsewhere [7, 16]. The Au(111) single crystal was cleaned by standard sputter-annealing procedures, followed by thermal deposition of either Pt-H or Pt-amyl from a Knudsen cell at about 480 K and 420 K, respectively, while keeping the Au substrate at room temperature. The sample was then transferred *in situ* into the cold STM (sample temperature 5 K). Topography images were taken in constant-current mode. For STS spectra, the differential conductance dI/dV was measured as a function of the sample bias V using the lock-in technique under open feedback conditions (typical modulation: 10–40 $\mathrm{mV_{rms}}$). Energy-resolved spectral maps were acquired by measuring dI/dV at fixed bias while scanning the surface in constant-current mode. For the DFT calculations of Pt-H, Kohn-Sham molecular orbitals were calculated

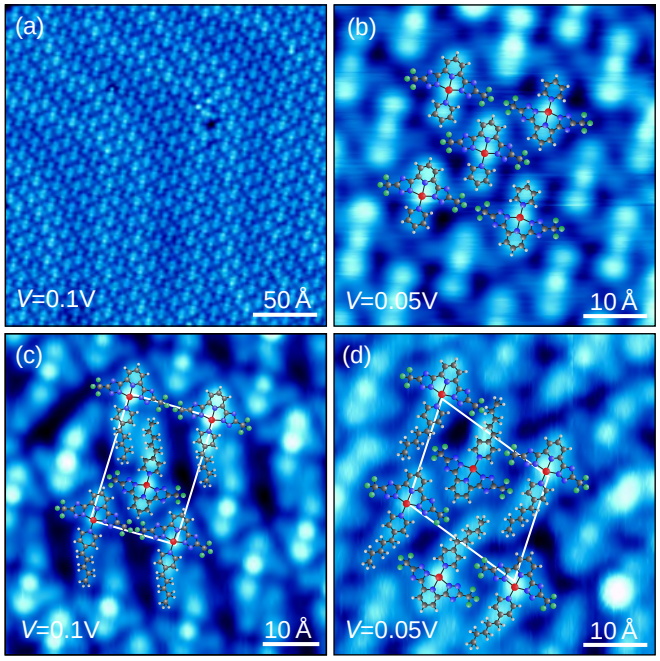

FIG. 1. (Color Online). (a,b) Overview and close-up STM image of the monolayer of Pt-H, respectively. (c,d) Close-up images of two different packing structures of Pt-amyl. While the presence of additional amyl groups in Pt-amyl lead to formation of pairs and an overall high degree of order, Pt-H exhibits randomly distributed parallel or antiparallel orientation (d). The overlaid molecular structure models demonstrate that the high spatial resolution enables an unambiguous identification of the molecules.

in the gas phase with the Gaussian 09 package using the B3LYP functional and the SDD basis set [17–19].

We first focus on the structural characterization of the as-grown molecular films. Figure 1 shows STM images of Pt-H (a,b) and Pt-amyl (c,d) on Au(111), respectively. We found that all molecules are intact and self-assemble in densely packed monolayer islands. The close-up views clearly show that the complexes can be imaged with submolecular resolution, permitting identification by a simple overlay of the structural models. The complexes consist of a platinum atom surrounded by a tridentate ligand (TL) and an ancillary ligand (AL) in square-planar coordination. The brightest feature is a round protrusion in the center of the complexes that we attribute to the Pt site. The TL shows up as an "arrow head" with two lobes to the left and right of the Pt site (stemming from the triazole-CF_3 groups) plus one above the Pt site (pyridine group). The two complexes only differ in the AL, being a pyridine in case of Pt-H and an amyl-pyridine for Pt-amyl. This difference can be distinguished in the STM images: the C_5H_11 group is seen as an additional "tail" in (c,d), whereas the bare pyridine in Pt-H only appears as a round protrusion (b).

From a comparison of the monolayer structures we can deduce the driving forces of self-assembly. Pt-H molecules are close-packed in a rhombic lattice with side length 11.5(3) Å and an angle of 86(4)° (b). However, the molecular orientation at each lattice point can either be parallel or antiparallel with respect to the neighboring molecules. We did not find any nearest or next-nearest neighbor correlations, i.e., the orientation is purely random. The molecular symmetry axis is 12.0(5)° rotated relative to the Au$\{11\bar{2}\}$ direction. While only one self-assembled pattern is found for Pt-H, we observed two different packings of Pt-amyl: at lower local coverage we found a rectangular unit cell containing two molecules (c); at a nominally full monolayer, we observed a denser oblique unit cell (d). The molecular symmetry axes relative to Au$\{11\bar{2}\}$ are 9(3)° in (c) as well as 4(3)° and 15(3)° in (d). We attribute the more complex self-assembly of Pt-amyl to additional van der Waals interactions between the amyl groups [20, 21]. On the other hand, the orientational variations in Pt-H lead us to conclude that there is no significant lateral interaction between the TLs of neighboring molecules and that the structural arrangement is simply a close-packing taking into account steric effects. Furthermore, the various molecular angles relative to the Au(111) substrate indicate that the molecule-substrate interaction is relatively weak.

Measurements of the differential conductance at different sites within individual molecules permits to understand the local electronic structure of the adsorbed Pt complexes, as dI/dV variations reflect the spatial local density of states (LDOS) distributions of molecular orbitals [8]. Figure 2 shows dI/dV spectra for Pt-H and Pt-amyl, respectively. While positions vary by some tens of mV for different molecules within the monolayer, peak widths are in the order of 100 mV. Apart from a systematic shift of about 0.1 eV, the spectra of Pt-H and Pt-amyl are very similar. Occupied states can be found at about -2 eV, mainly localized at the TL-triazole groups. Unoccupied states are observed above about +2 eV at the TL-pyridine group.

In order to connect the observed spatial LDOS variations to specific molecular orbitals, we performed energy-resolved spectroscopic mapping. As we found almost identical spectroscopic results for both molecules, we restrict our discussion to Pt-H. We measured dI/dV maps over a wide range from -3.2 V to +3.2 V. Figure 3 summarizes maps at energies where we found contributions from the ligand (i.e. not the Pt site). In order to correlate the observed features with specific sites of the complex, the maps are superimposed with molecular structures. We first describe the unoccupied region. At voltages from 3.1 V down to 2.3 V, maps show strong intensities at the left- and right-hand sides of the TL-pyridine group of each molecule (Fig. 3a). This is in accordance with the spatial localization of the shoulder at 2.6 V in STS spectra. Within the molecular layer, the highest in-

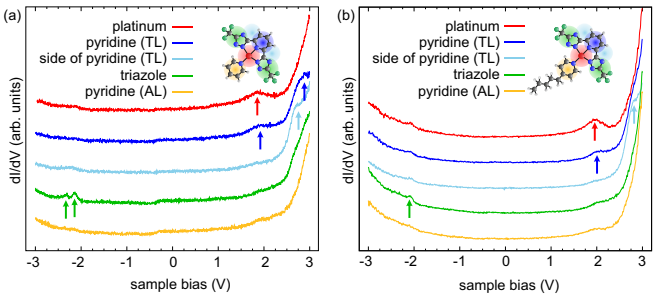

FIG. 2. (Color Online). Local tunneling spectra of Pt-H (a) and Pt-amyl (b) on Au(111). The spectra where taken over the different parts of the molecule as indicated by the color code of the molecular model. The arrows indicate features caused by molecular orbitals.

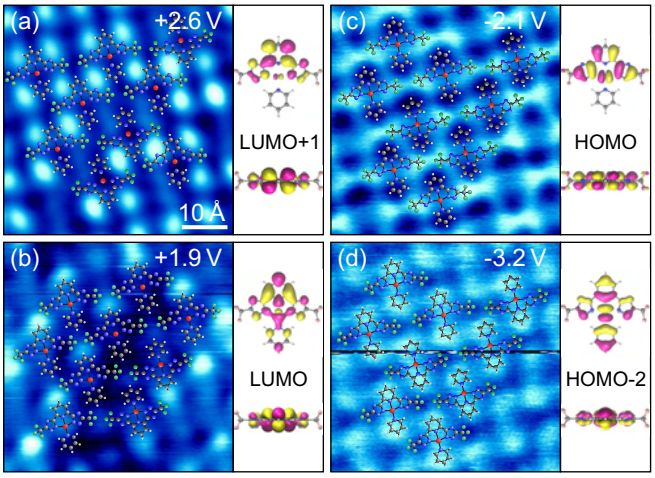

FIG. 3. (Color Online). Series of dI/dV maps exhibiting LDOS at the ligands and assignment of corresponding calculated orbitals of the gas-phase molecule. The unoccupied states mainly show LDOS contributions from the TL-pyridine (a,b), while the HOMO is localized at the triazole groups (c). The HOMO–2 exhibits LDOS at both TL- and AL-pyridines. Note that the maps shown in (a,b) have been acquired at a different position compared to those in (c,d).

tensities are found in regions between two neighboring TL-pyridines and significantly low intensity between two ALs. This proves that the dominating signal stems from TL rather than the AL. The lack of intensity at the center of the TL-pyridine suggests that the underlying orbital exhibits a node in the mirror plane of this group. At bias voltages below 2.3 V and ranging down to 1.6 V (b), we observe a feature above the center of the TL-pyridine groups, while no signal is found at the TL-triazoles or the ALs. Thus, unoccupied ligand states are mainly confined to the TL-pyridine group. In the occupied region, dI/dV intensity is found at the TL-triazole groups over a wide energy range from -1.8 V to -2.9 V, whereas the pyridine groups of both TL and AL have almost no intensity (c). This behavior is in good agreement with the spatial inhomogeneity of peaks below -2.0 V in the tunneling spectra. Below -3.0 V, the dI/dV maps appear to be inverted as intensity is now located at both AL- and TL-pyridine groups but not at the triazoles (d).

The energy-resolved spectral maps can be assigned to particular molecular orbitals via comparison with calculated orbitals of the complex in the gas phase, as seen in Fig. 3. The lowest unoccupied molecular orbitals (LUMO and LUMO+1) are mainly localized at the TL-pyridine group. While the LUMO is symmetric with respect to the molecular mirror plane (b), the LUMO+1 is antisymmetric (a). As the same symmetry is also found in the dI/dV maps at about 2.0 V and 2.6 V, respectively, we assign the observed features to the LUMO and LUMO+1, as shown in Fig. 3 [22]. The calculated energy separation of 0.65 eV for the gas-phase molecule is in good agreement with the experimentally observed 0.7 eV. The calculated highest occupied molecular orbital (HOMO) is mainly distributed across the triazole groups of the TL. DFT predicts the HOMO-LUMO gap to be 3.88 eV, which again agrees well with the peak separation of about 4 eV in the tunneling spectra (Fig. 2). The occupied spectroscopic map in Fig. 3d shows very good correspondence with the calculated HOMO–2 that lies 0.68 eV lower than the HOMO. Overall, the comparison shows that we can assign molecular orbitals to each of the dI/dV maps. We found that occupation, order and energy separation of the calculated ligand orbitals in the gas phase are in good agreement with the measured orbitals of the adsorbed complex, i.e., the molecular properties at the ligand remain essentially unchanged upon adsorption to the Au surface, again indicating an overall weak molecule-substrate interaction.

The situation is different when we look at the Pt site of the complex. The DFT calculations show that the HOMO–1 is a d_{z^2} orbital highly localized to the Pt atom (Fig. 4). However, no increased spectroscopic intensity is found at the Pt atom in any of our dI/dV maps below -2.0 V. Instead, we observe a spectroscopic feature with increased LDOS intensity at the Pt atom and no contributions from the ligand in maps between -1.4 and -0.4 V (Fig. 4a). Between -0.3 and 1.0 V, dI/dV maps resemble the topography (b), which is a typical observation for tunneling in the region of the HOMO-LUMO gap of an adsorbed molecule (i.e. no resonant tunneling into a distinct molecular orbital occurs). Unexpectedly, we also found LDOS intensity localized at the Pt atom in the unoccupied region between 1.0 and 1.8 V (c). At first glance, this observation is surprising, because there can only be one d_{z^2} orbital at the Pt atom, and the calculations of the gas-phase molecule predict it to be a fully occupied HOMO–1.

The modified electronic behavior of the complex at its Pt site can be understood in terms of site-specific local-

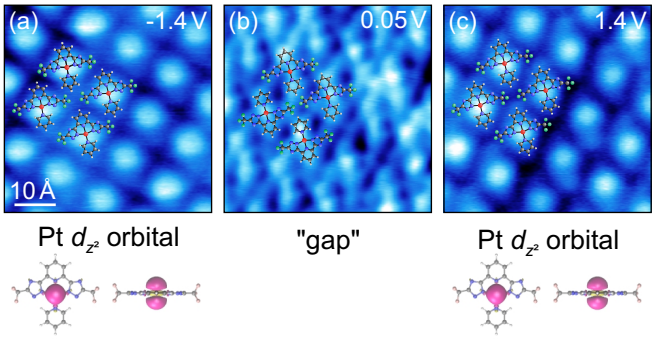

FIG. 4. (Color Online). dI/dV maps within the energy windows -1.4 to 0.4 eV (a) and 1.0 to 1.8 eV (c) show localized LDOS at the Pt atom. In between, the maps resemble the topography (b), typical for a gap region. DFT predicts an occupied Pt d_{z^2}-state for the gas-phase molecule. Its experimental observation both below and above E_F is indicative of a partially depopulated orbital.

ized molecule-substrate interaction and charge transfer. As can be seen in the side view of the calculated molecular orbitals in Fig. 3 and 4, the Pt d_{z^2}-orbital extends out of the molecular plane farther than the ligand orbitals. Therefore, locally increased overlap with metallic states from the Au substrate can be expected at the Pt site. Molecule-substrate hybridization can lead to a shift in binding energy as well as a broadening of the d_{z^2} state. Strong overlap with the metallic substrate can also induce charge transfer. We observed two orbitals at the Pt atom with identical spatial distribution within the energy windows -0.9 ± 0.5 eV and 1.5 ± 0.5 eV, respectively. This behavior has been observed for the case of a singly occupied molecular orbital (SOMO) [23]: at positive sample bias, a second electron can tunnel into the SOMO as soon as the energy is large enough to overcome the on-site Coulomb repulsion. This way, the SOMO is detected both below and above the Fermi energy E_F. Typical Coulomb energies for d_{z^2} states in organometallic molecules are around 2 eV [24–26], in accordance with the 2.4 ± 0.7 eV observed here. Another scenario for our observation can be the formation of a bonding and an antibonding state due to strong hybridization of the Pt d_{z^2}-orbital with Au states [27]. This latter possibility can also explain why we do not observe these states as peaks in our tunneling spectra.

At this point, we cannot distinguish between those two possibilities. However, in both cases, the transfer of an electron from the molecule to the substrate is required. Thus, we conclude that the d_{z^2} orbital of the Pt complex is only partially occupied when adsorbed on the Au(111) surface. In contrast, the ligand orbitals of the adsorbed molecule are unaffected by the adsorption onto the Au surface. This means that charge transfer of an electron between the molecule and the substrate only occurs through the Pt atom, while the molecule-substrate interaction via the ligand is small. We emphasize that our analysis of electronic properties is identical for all complexes within the monolayer, i.e., the molecules interact in a well-defined way with the substrate. This is only possible due to its planar structure that leads to distinct orbital overlaps. Hence, we expect that well-defined interaction also occurs in host-guest environments as well as within aggregated structures of Pt(II) complexes. This interaction should even be tunable in a controlled fashion by systematic variation of the ligand side groups (e.g., replacing CF_3 by tert-butyl or adamantyl [7]) or by changing the host or substrate material [10, 28].

In summary, we have shown that Pt(II) complexes can be thermally sublimated without any visible fragmentation, and they self-assemble into well-ordered monolayers. STM and STS experiments were able to probe the real-space and electronic structure with submolecular resolution. The orbital structure of the ligands remains essentially unaltered by the presence of the Au(111) surface. However, the strongly changed electronic structure at the Pt atom provides evidence for a localized charge transfer. These findings show that – contrary to the commonly used Ir(III) complexes – planar Pt(II) complexes exhibit a well-defined directional interaction with their local environment that offers the opportunity of engineering their electronic and thereby also optical properties.

This work was supported by the Deutsche Forschungsgemeinschaft (DFG) through project WE-4104/2-1 and the Transregional Collaborative Research Center TRR 61, project B13.

* ca.s@uni-muenster.de
† daniel.wegner@uni-muenster.de

[1] K. Müllen and U. Scherf, eds., *Organic Light-Emitting Devices* (Wiley-VCH, Weinheim, 2006).
[2] M. A. Baldo, D. O'Brien, A. Shoustikov, S. Sibley, M. E. Thomson, and S. R. Forrest, Nature **395**, 151 (1998).
[3] H. Yersin, ed., *Highly Efficient OLEDs with Phosphorescent Materials* (Wiley-VCH, Weinheim, 2007).
[4] L. Flamigni, A. Barbieri, C. Sabatini, B. Ventura, and F. Barigelletti, Top. Curr. Chem. **281**, 143 (2007).
[5] S. Reineke, G. Schwartz, K. Walzer, M. Falke, and K. Leo, Appl. Phys. Lett. **94**, 163305 (2009).
[6] C. A. Strassert, C.-H. Chien, M. D. Galvez Lopez, D. Kourkoulos, D. Hertel, K. Meerholz, and L. De Cola, Angew. Chem. Int. Ed. **50**, 946 (2011).
[7] M. Mydlak, M. Mauro, F. Polo, M. Felicetti, J. Leonhardt, G. Diener, L. De Cola, and C. A. Strassert, Chem. Mater. **23**, 3659 (2011).
[8] X. Lu, M. Grobis, K. H. Khoo, S. G. Louie, and M. F. Crommie, Phys. Rev. Lett. **90**, 096802 (2003).
[9] J. Repp, G. Meyer, S. M. Stojković, A. Gourdon, and C. Joachim, Phys. Rev. Lett. **94**, 026803 (2005).
[10] D. Wegner, R. Yamachika, Y. Wang, V. W. Brar, B. M. Bartlett, J. R. Long, and M. F. Crommie, Nano Lett. **8**,

131 (2008).
[11] H. Kim, W.-j. Son, W. J. Jang, J. K. Yoon, S. Han, and S.-J. Kahng, Phys. Rev. B **80**, 245402 (2009).
[12] A. Weber-Bargioni, W. Auwärter, F. Klappenberger, J. Reichert, S. Lefrançois, T. Strunskus, C. Wöll, A. Schiffrin, Y. Pennec, and J. V. Barth, ChemPhysChem **9**, 89 (2008).
[13] N. Oncel and S. L. Bernasek, Appl. Phys. Lett. **92**, 133305 (2008).
[14] H. Gersen, R. Schaub, W. Xu, I. Stensgaard, E. Laegsgaard, T. R. Linderoth, F. Besenbacher, M. K. Nazeeruddin, and M. Graetzel, Appl. Phys. Lett. **89**, 264102 (2006).
[15] Z. Ng, K. P. Loh, L. Li, P. Ho, P. Bai, and J. H. K. Yip, ACS Nano **3**, 2103 (2009).
[16] L. De Cola, C. A. Strassert, M. Mathias, M. Mauro, M. Felicetti, G. Diener, and J. Leonhardt, Patent DE102011001007 (2012).
[17] Gaussian 09, Revision A.1, M. J. Frisch et al., Gaussian, Inc., Pittsburgh PA, 2009.
[18] A. D. Becke, J. Chem. Phys. **98**, 5648 (1993).
[19] D. Andrae, U. Häußermann, M. Dolg, H. Stoll, and H. Preuss, Theor. Chem. Acc. **77**, 123 (1990).
[20] X. Qiu, C. Wang, S. Yin, Q. Zeng, B. Xu, and C. Bai, J. Phys. Chem. B **104**, 3570 (2000).
[21] S. Furukawa, K. Tahara, F. C. De Schryver, M. Van der Auweraer, Y. Tobe, and S. De Feyter, Angew. Chem. Int. Ed. **46**, 2831 (2007).
[22] The dI/dV signal appears to be located next to rather than at the molecule. This is merely an artifact when scanning in constant-current mode.
[23] J. Repp, G. Meyer, S. Paavilainen, F. E. Olsson, and M. Persson, Science **312**, 1196 (2006).
[24] A. Zhao, Q. Li, L. Chen, H. Xiang, W. Wang, S. Pan, B. Wang, X. Xiao, J. Yang, J. G. Hou, and Q. Zhu, Science **309**, 1542 (2005).
[25] T. Lukasczyk, K. Flechtner, L. R. Merte, N. Jux, F. Maier, J. M. Gottfried, and H.-P. Steinrück, J. Phys. Chem. C **111**, 3090 (2007).
[26] A. Mugarza, R. Robles, C. Krull, R. Korytár, N. Lorente, and P. Gambardella, Phys. Rev. B **85**, 155437 (2012).
[27] R. Hoffmann, Rev. Mod. Phys. **60**, 601 (1988).
[28] H. Harutyunyan, M. Callsen, T. Allmers, V. Caciuc, S. Blügel, N. Atodiresei, and D. Wegner, Chem. Commun. **49**, 5993 (2013).